Cirrus Cloud Microphysical Property Retrieval Using Lidar and Radar Measurements. Part II: Midlatitude Cirrus Microphysical and Radiative Properties

ZHIEN WANG AND KENNETH SASSEN

Department of Meteorology, University of Utah, Salt Lake City, Utah

(Manuscript received 11 May 2001, in final form 18 January 2002)

ABSTRACT

The lidar–radar algorithm described in Part I of this set of papers is applied to ~1000 h of Raman lidar and millimeter wave cloud radar (MMCR) data collected at the Atmospheric Radiation Measurement program Southern Great Plains Clouds and Radiation Testbed site in Oklahoma during the period from November 1996 to November 2000. The resulting statistics of cirrus microphysical and radiative properties show that most cirrus clouds are optically thin (mean optical depth of 0.58 with a standard deviation of 0.67) with low ice water path (mean 12.19 g m^{-2} with a standard deviation of 19.0). The seasonal changes of cirrus properties are relatively small except for the general effective radius (D_{ge}). Strong temperature dependencies of ice water content, D_{ge}, and extinction coefficients are found in the dataset, which are well described by second-order polynomial functions. The temperature and thickness dependencies of the cirrus properties are studied in detail, providing information useful in the validation and improvement of cirrus parameterizations in general circulation models. The limitations of the MMCR for cirrus detection are also considered through comparisons with results from the Raman lidar, which show that the MMCR fails to detect most thin cirrus with $\tau \leq 0.1$ and consistently underestimates physical cloud thickness. Comparisons with available data describing cirrus microphysical and radiative properties are made, and an improved cirrus particle extinction coefficient parameterization based on the combined lidar–radar approach is offered.

1. Introduction

Accurate parameterizations of cirrus cloud properties in general circulation models (GCMs) are important in evaluating the prospects for climate change. The studies of Lohmann and Roeckner (1995) using different cirrus emissivities illustrate that cirrus clouds are likely to play a crucial role in regulating global climate sensitivity. Currently, cloud properties are parameterized in GCMs as a function of a set of resolved dynamic and thermodynamic properties (McFarlane et al. 1992; Tiedtke 1993; Fowler et al. 1996; Del Genio et al. 1996). Because of the poorly understood interactions between clouds and the hydrological cycle, and the multiscale nature of cloud formation and microphysical processes, different cloud parameterizations in GCMs appear to produce a threefold variation in the predicted magnitudes of global surface temperature change resulting from more abundant greenhouse gases (Cess et al. 1990).

The radiative effects of cirrus depend strongly on cloud microphysical properties (Liou 1986; Stephens et al. 1990), which, unfortunately, are still poorly known. The studies of Fu (1996) suggest that the radiative properties of cirrus can be parameterized as functions of two variables, ice water content (IWC) and the general effective radius D_{ge} of the ice particles. Providing cloud macrophysical and microphysical property datasets to test and improve cloud parameterizations in GCMs is a priority in current climate change research. The U.S. Department of Energy's Atmospheric Radiation Measurement (ARM) program (Stokes and Schwartz 1994) is trying to achieve this goal with extensive long-term surface observations at multiple Cloud and Radiation Testbed (CART) sites.

Recent research at the University of Utah Facility for Atmospheric Remote Sensing (FARS; Sassen et al. 2001) has involved the development of improved single and multiple remote sensor cloud property retrieval algorithms, especially with regard to the similar set of passive and active instruments at the FARS and CART sites. Using such a combination of instruments, Wang and Sassen (2001) reported statistical results of cloud type and other properties. In the first part of this set of papers (Wang and Sassen 2002, hereafter Part I), we presented a method that relies on the cloud extinction coefficient (σ) derived from lidar measurements and the water equivalent radar reflectivity factor (Z_e) from cloud radar measurements to retrieve IWC and D_{ge}. Here in Part II, the algorithm is applied to Raman lidar and millimeter-wave cloud radar (MMCR) data collected at

Corresponding author address: Zhien Wang, GEST Center, NASA GSFC, Mail Code 912, Bldg. 33, Rm. A417, Greenbelt, MD 20771. E-mail: zhien@agnes.gsfc.nasa.gov

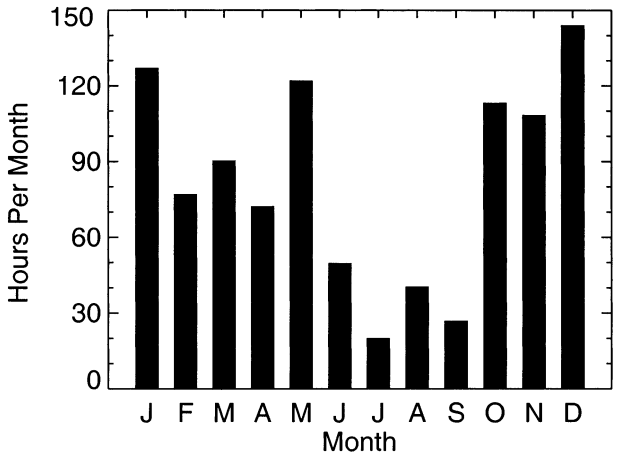

FIG. 1. Hours of observations in each month for the SGP CART cirrus samples used in this study.

the Southern Great Plains (SGP) CART site in Oklahoma (36.605°N, 97.485°W), leading to the derivation of basic statistics of cirrus microphysical and radiative properties. Using this dataset the dependencies of these midlatitude cirrus cloud properties with temperature and cloud layer thickness are examined and compared with results from other sites.

2. The CART dataset

In this study we analyze ~1000 h of combined Raman lidar (Goldsmith et al. 1998) and MMCR (Moran et al. 1998) measurements collected at the SGP CART site over the period from November 1996 to November 2000 using our lidar–radar algorithm (see Part I). The MMCR is a zenith-pointing radar that operates at 34.86 GHz (8.7-mm wavelength). It has a 2-m diameter dish and a sensitivity of about −50 dBZ (10 logZ_e) at 5.0-km range. This unique cloud radar, operating in cycles through four data collection modes with selectable parameters, can detect most tropospheric clouds from stratus to cirrus with a vertical resolution of 45 or 90 m. The radar also possesses a Doppler capability that allows the measurement of cloud constituent vertical velocities.

The CART Raman lidar transmits at 0.355 μm and receives the elastic backscatter signal at 0.355 μm in both polarization planes, as well as the Raman backscatter signals at 0.387 and 0.408 μm (Goldsmith et al. 1998). These latter wavelengths correspond to Raman-shifted scattering from nitrogen and water vapor molecules, respectively. Received signals are split into a short-range wide field-of-view (typically 3 mrad) channel (~5%) and a long-range narrow field-of-view (typically 0.3 mrad) channel (~95%), normally allowing the system to have enough dynamic range to detect signals from the entire troposphere. This dual field-of-view design also provides excellent daytime capability without sacrificing nighttime performance.

In addition to providing information describing the vertical profiles of water vapor and aerosols (Ferrare et al. 1998), the CART Raman lidar is also useful in deriving cloud optical properties. Independent height profiles of cirrus cloud backscattering and extinction coefficients, extinction-to-backscatter ratio, and linear depolarization ratio (δ) are calculated from the elastic backscatter signal at 0.355 μm, the corresponding nitrogen Raman backscattering signal at 0.387 μm, and standard or measured atmospheric sounding profiles (Ansmann et al. 1992).

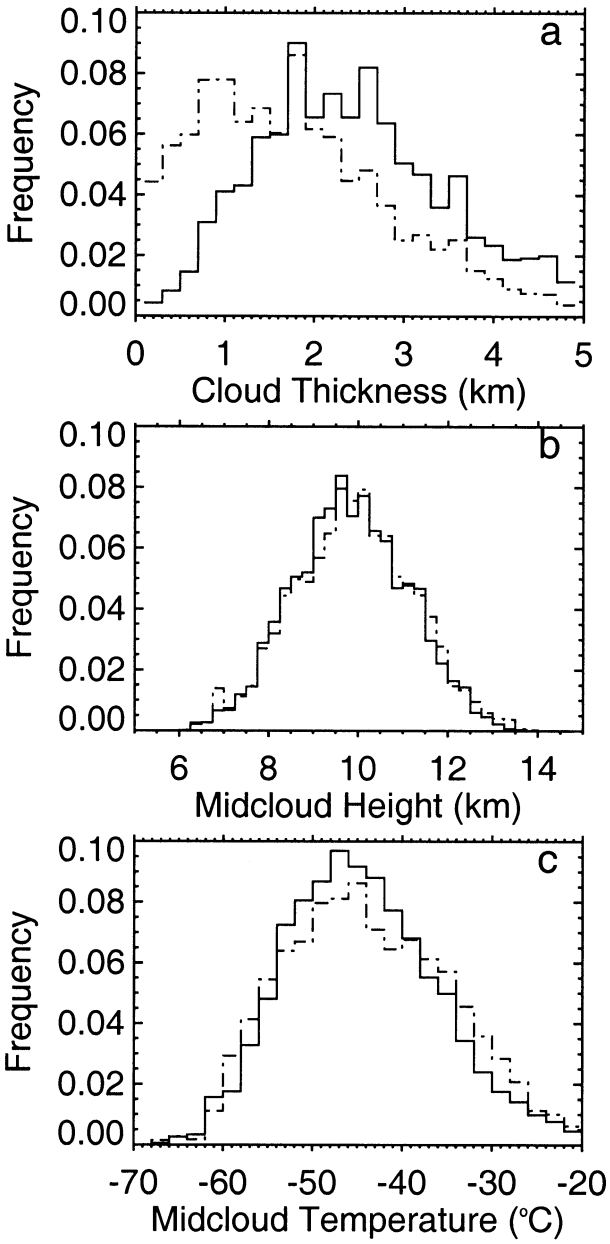

FIG. 2. Frequency distributions of (a) cloud layer thickness, (b) midcloud height, and (c) midcloud temperature derived from the MMCR (dashed line) and Raman lidar (solid line) for the 4-yr cirrus cloud dataset at the SGP CART site.

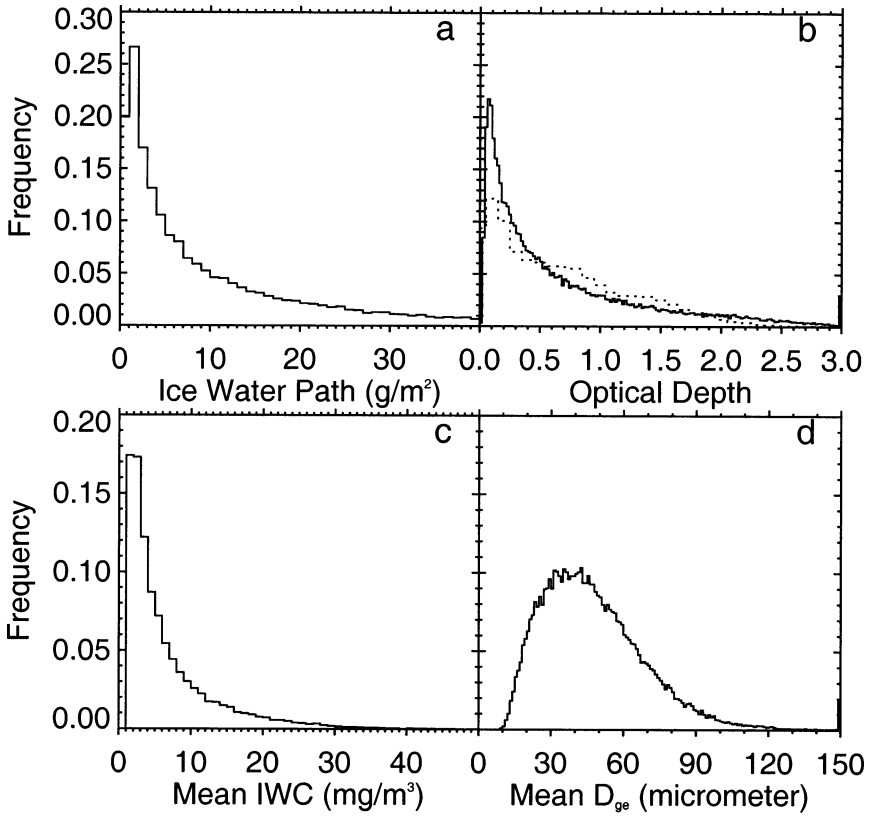

FIG. 3. Frequency distributions of (a) IWP, (b) τ, (c) layer-mean IWC, and (d) layer-mean D_{ge}. The statistics for cirrus cloud τ at FARS is shown in (b) as the dashed line.

The Raman lidar technique is a powerful tool for cirrus studies because more accurate σ profiles can be derived than those from lidar measurements based solely on the elastic channel. We derive cirrus cloud σ using a method similar to that used by Ansmann et al. (1992). When the signal in the Raman channel is too noisy for the analysis of the whole cloud layer, we retrieve the cloud extinction profile from the elastic channel with an average extinction-to-backscatter ratio derived from the Raman channel in the lower cloud portion and/or with the constraint of total optical depth (Young 1995). To improve the signal-to-noise ratio of the lidar signal, a 10-min sliding average is applied to the Raman lidar data. The effect of multiple scattering on σ retrieval is not considered in this study, and this may cause the underestimation of visible cloud optical depth (τ) and average σ. However, we consider this effect as not very significant for high cloud observations because of the narrow field of view.

In our study cirrus clouds are identified according to cloud-base height and δ value constraints. Clouds are classified as cirrus provided that the minimum $\delta > 0.1$ and mean cloud base altitude is $>$7.0 km over the observation period (see Wang and Sassen 2001). Although we recognize that this dataset may include some ice-phase altostratus clouds, a comparison of a subset of derived and visually identified cirrus clouds indicates that this is not a significant problem, so we refer to the dataset as cirrus clouds. Due to the strong lidar attenuation generated by many low and middle clouds, most cirrus clouds in our sample involve single-layer cloud systems.

The monthly distribution of observation hours in the dataset is illustrated in Fig. 1. In comparison with other high cloud occurrence statistics at the SGP CART site (Wang and Sassen 2001; Mace et al. 2001), cirrus clouds in summer season are under sampled in this dataset because of more limited Raman lidar observations in this season. Because of the different sensitivities of lidars and radars, radars often do not detect thin cirrus clouds or parts of the cirrus detected by the Raman lidar. The cloud thickness (ΔZ) frequency distribution for the cirrus sample detected by both the lidar and radar is shown in Fig. 2a. From this figure, we can see that even the MMCR, one of the most sensitive cloud radars extant, will not detect parts of cirrus clouds, thus resulting in an underestimation of ΔZ. Cirrus cloud microphysical properties are derived in this study only for the portion of cirrus detected by both the lidar and radar, so it should be recognized that these results will neglect some thin cirrus clouds.

Frequency distributions of cirrus midcloud height and

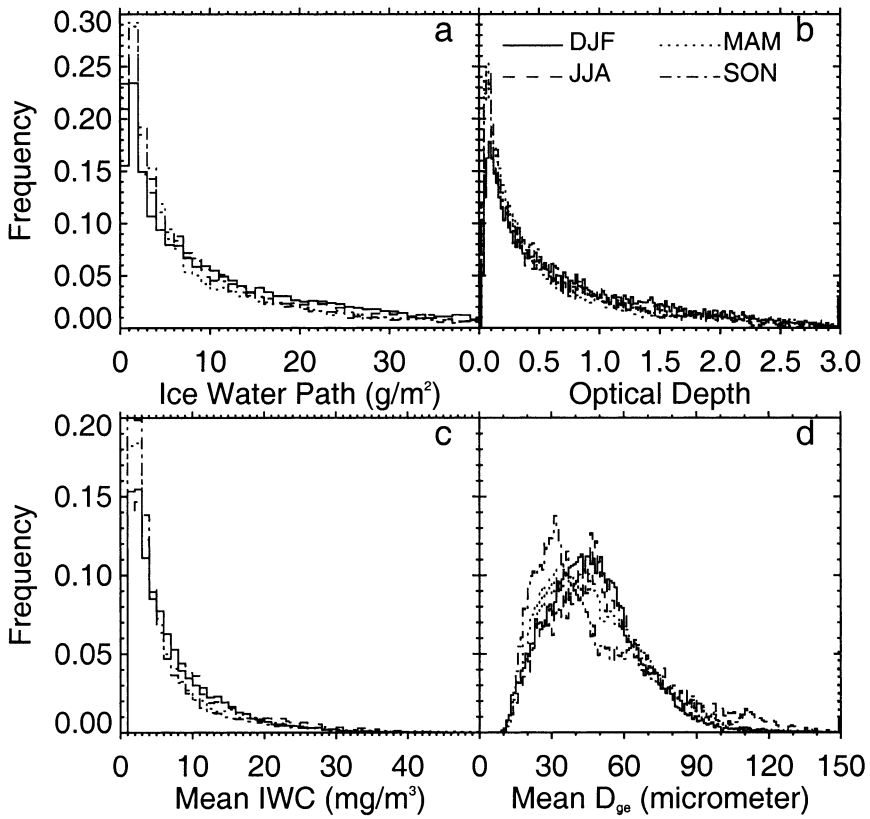

FIG. 4. As in Fig. 3, except for different seasons.

temperature (T_m) derived from the MMCR and Raman lidar individually are given in Figs. 2b and 2c. From these displays we can see that the maxima in the distributions occur ~10.0 km and at ~−45°C. Although there is a significant bias in the ΔZ frequency distribution from MMCR measurements compared with the Raman lidar, the biases in midcloud height and T_m are small.

3. Statistics of cirrus microphysical and radiative properties at the SGP site

The lidar–radar algorithm presented in Part I is applied to the dataset described above. Potential errors in IWC and D_{ge} come from measurement errors in σ and Z_e, and parameterization errors in expressing σ and Z_e as functions of IWC and D_{ge}. The error analysis in Part I shows that the error in D_{ge} is smaller than the error in IWC for a given error in Z_e, σ, and their parameterizations. The algorithm has good tolerance for the measurement errors in Z_e and its parameterization error. The accuracy of IWC is strongly dependent on the accuracy of σ and its parameterization. The parameterization of σ as a function of IWC and D_{ge} has good accuracy (Fu 1996), and the Raman lidar measurements provide reliable σ. Thus we believe that there is no significant systematic error in IWC and D_{ge} from σ and its parameterization. The parameterization of Z_e as a function of IWC and D_{ge} may introduce systematic errors due to several assumptions. However, IWC and D_{ge} are less sensitive to errors in Z_e and its parameterization, than to error in σ and its parameterization. For example, a 50% error in Z_e parameterization only results in less than 15% error in IWC and D_{ge}. Because of the strong variability of cirrus particle shape and size distribution, the error in Z_e parameterization is most likely a random error, while the systematic error is small. The MMCR at the SGP CART site is a well calibrated operational cloud radar. Calibration error of 1 dBZ results only in a <8% systematic error in IWC and D_{ge}. Therefore, the systematic error in IWC and D_{ge} is estimated to be better than 15%. The random error in IWC and D_{ge} can be larger for a given data point, but this source error can be reduced by accumulating large samples.

Using the ~1000 h of SGP CART data retrievals, we provide in Fig. 3 the frequency of occurrence distributions of ice water path (IWP), τ, layer-mean IWC, and D_{ge}. The frequency of occurrence distribution of τ from FARS data is shown as the dashed line in Fig. 3b for comparison. All FARS cirrus statistics used for comparisons in this paper are reported in Sassen and Comstock (2001) and are derived from the combined lidar and infrared radiometer (LIRAD) method (Platt et al. 1987; Comstock and Sassen 2001). Most cirrus clouds

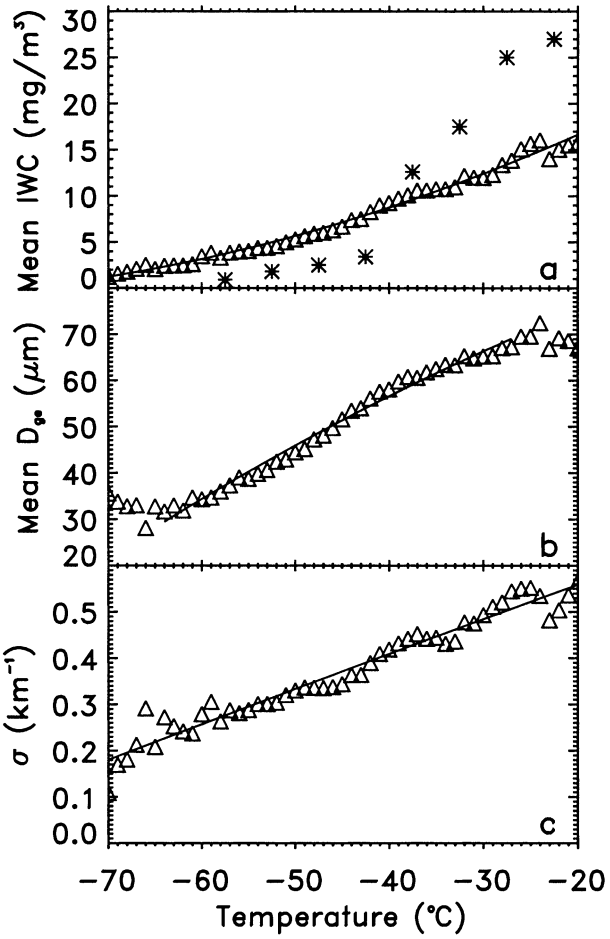

FIG. 5. Temperature dependencies of (a) mean IWC, (b) mean D_{ge}, and (c) σ from the SGP CART cirrus cloud dataset, compared with the temperature dependency of IWC from Heymsfield and Platt (1984; asterisks).

in our midlatitude sample are optically thin with relatively low IWP or mean IWC. The mean of τ is 0.58 with a standard deviation of 0.67, while the mean IWP is 12.19 g m^{-2} with a standard deviation of 19.0. These mean values are generally consistent with other results (Mace et al. 2001; Sassen and Comstock 2001). Note that the maximum in the D_{ge} distribution (Fig. 3d) is located at ~40 μm.

The above statistics are broken into different seasons [December–February (DJF), March–May (MAM), June–July (JJA), September–November (SON)] in Fig. 4. Except for the frequency distributions of D_{ge}, the results are similar for the different seasons. This feature suggests that the sample bias in summer season should not cause serious problems in the statistics. During the SON season, the modal particle size is ~30 μm, which is smaller than for other seasons (~40–60 μm). Note that there are more cirrus with large particles in the JJA season, which is probably due to more cirrus clouds related to thunderstorm, or deep convective, formation processes.

TABLE 1. The mean and standard deviation of IWC, D_{ge}, and σ at different temperatures. Values in parentheses denote std dev.

T (k)	IWC (mg m^{-3})	D_{ge} (μm)	σ (km^{-1})
−20.0	15.73 (22.69)	66.98 (40.53)	0.566 (0.698)
−22.0	15.05 (22.75)	69.19 (42.11)	0.504 (0.550)
−24.0	16.05 (21.31)	72.46 (44.99)	0.535 (0.557)
−26.0	15.10 (18.57)	69.52 (48.62)	0.550 (0.593)
−28.0	13.38 (16.72)	67.05 (42.72)	0.521 (0.547)
−30.0	11.99 (14.62)	65.21 (40.02)	0.493 (0.533)
−32.0	12.19 (15.62)	65.27 (37.49)	0.478 (0.493)
−34.0	10.75 (14.02)	63.40 (35.72)	0.431 (0.431)
−36.0	10.61 (13.87)	61.76 (38.30)	0.442 (0.452)
−38.0	10.09 (12.17)	60.77 (39.80)	0.442 (0.452)
−40.0	9.25 (10.88)	58.08 (32.60)	0.419 (0.427)
−42.0	8.27 (9.52)	56.08 (29.48)	0.390 (0.395)
−44.0	7.40 (8.11)	53.44 (27.06)	0.364 (0.344)
−46.0	6.31 (7.05)	49.71 (26.38)	0.338 (0.316)
−48.0	5.91 (6.84)	47.26 (24.46)	0.336 (0.318)
−50.0	5.29 (6.31)	44.45 (23.55)	0.330 (0.343)
−52.0	4.59 (5.29)	42.44 (21.94)	0.304 (0.308)
−54.0	4.38 (5.18)	39.78 (20.60)	0.301 (0.309)
−56.0	3.98 (5.00)	38.99 (20.76)	0.281 (0.305)
−58.0	3.31 (4.20)	36.02 (18.78)	0.263 (0.302)
−60.0	3.46 (4.98)	34.32 (18.19)	0.279 (0.321)
−62.0	2.48 (2.41)	31.86 (15.85)	0.242 (0.242)
−64.0	2.43 (2.62)	31.70 (16.07)	0.272 (0.354)
−66.0	2.53 (2.59)	28.16 (13.53)	0.291 (0.387)
−68.0	1.77 (1.60)	32.81 (14.31)	0.181 (0.257)
−70.0	1.25 (0.85)	35.56 (12.64)	0.109 (0.101)

4. Temperature and thickness dependencies of cirrus microphysical and radiative properties

To improve cloud parameterizations in GCMs, one must know how cirrus cloud microphysical and radiative properties depend on other parameters associated with cloud processes. Various studies (Heymsfield and Platt 1984; Platt and Harshvardhan 1988; Sassen and Comstock 2001) have shown that temperature is an important factor in determining cirrus cloud properties because of the strength of the adiabatic process. Platt et al. (1987), Mace et al. (2001), and Sassen and Comstock (2001) have also shown that physical cloud thickness is another important factor influencing cirrus properties. Thus, we explore in some detail the temperature and thickness dependencies of cirrus properties using our extensive dataset.

a. Temperature dependency

The temperature dependencies of mean IWC, D_{ge}, and σ are illustrated in Fig. 5. We have related the retrieved cirrus properties to air temperature by using the nearest

TABLE 2. The second-order polynomial function constants for the temperature dependencies of IWC, D_{ge}, and σ.

	a	b	c
IWC	26.87	0.569	0.002 892
D_{ge}	90.14	0.659	−0.004 505
σ	0.7072	0.007 36	−2.379E−06

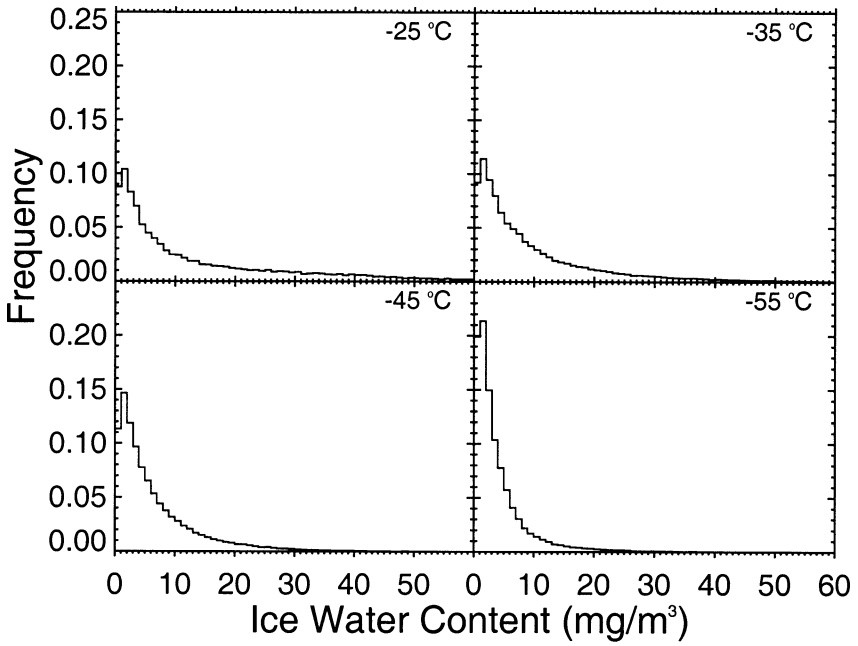

FIG. 6. Frequency distributions of IWC at selected temperatures within 3°C temperature bins.

CART upper air sounding. The mean and standard deviation of these quantities are calculated within 1.0°C bins and are given in Table 1. Clearly, mean IWC, D_{ge}, and σ increase monotonically with increasing cloud temperature, and we use a second-order polynomial function in temperature T (°C) to model them, that is, $a + bT + cT^2$, where a, b, and c are constants. The fitted results are both given in Table 2 and plotted in the figures as solid lines within the data range used for fitting.

Note that the results at temperatures less than approximately −60°C begin to deviate from the second-order polynomial fits. Because the MMCR fails to detect most optically thin cirrus at these cold temperatures, the samples are biased either to more optically thick cirrus or to cirrus with larger particles. Thus the statistics at

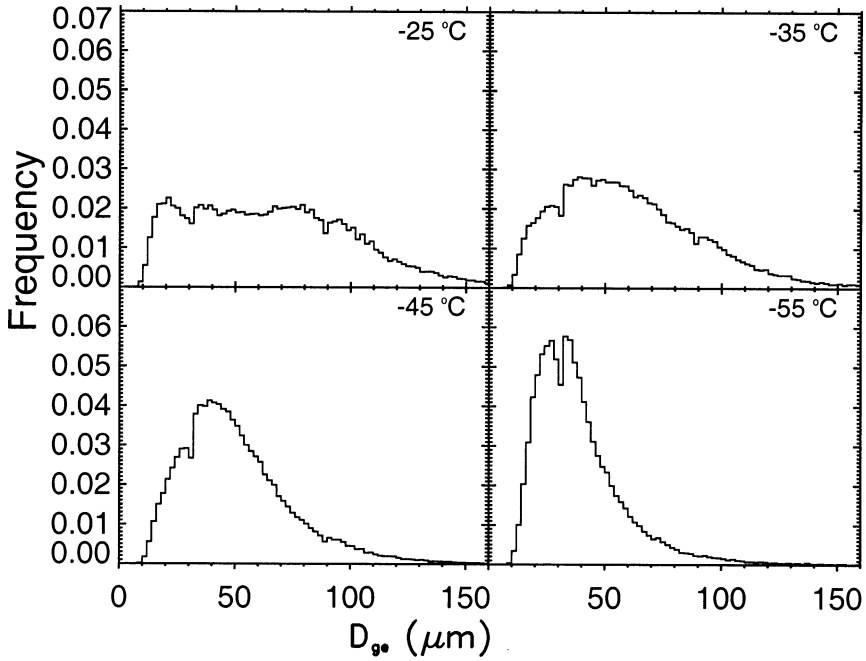

FIG. 7. As in Fig. 6, except for D_{ge}.

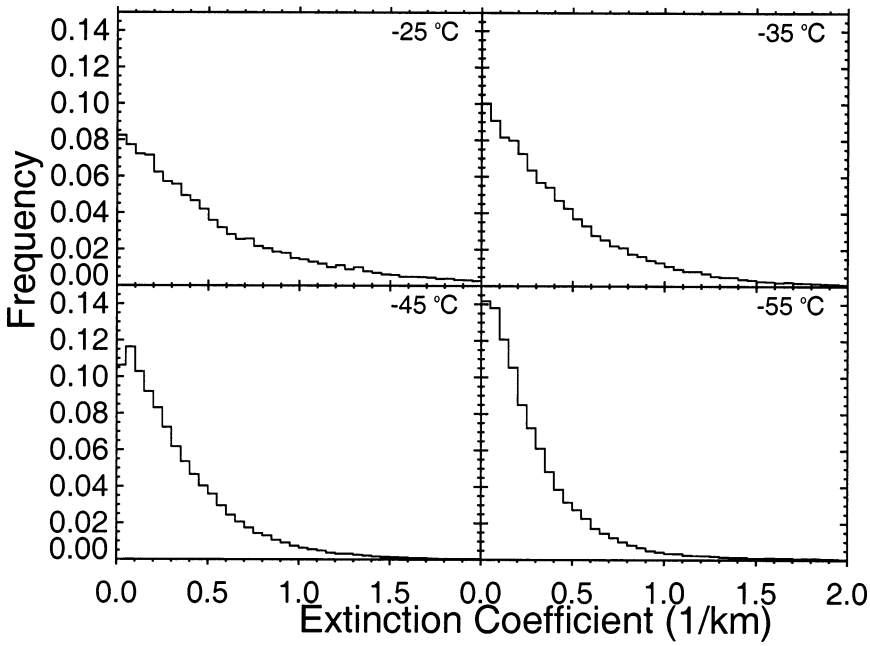

FIG. 8. As in Fig. 6, except for σ.

low temperatures shown in Fig. 5 are biased because of the sample bias in the lidar–radar algorithm. The effect of this sample bias will be discussed more in section 5. Nonetheless, these basic temperature tendencies are related to fundamental cirrus cloud microphysical processes (see, e.g., Khvorostyanov and Sassen 1998).

For comparison purposes, the temperature dependency of IWC from aircraft observations (Heymsfield and Platt 1984) is also included in Fig. 5a. The obvious differences between the two sets of results in Fig. 5a may have resulted from sampling different cloud types. The aircraft data shown in the figure are derived from relatively uniform and deep winter and springtime ice cloud, some of which may not be classified as cirrus. The differences can also probably be attributed to the limitations of the in situ probes used in Heymsfield and Platt (1984). For example, uncertainties in IWC estimated from 2D-C data can result from the relatively small sample volume and particle size limitation of this in situ probe.

From the standard deviations given in Table 1, one can see that cirrus microphysical and radiative properties vary widely for a given temperature. The frequency distributions of IWC, D_{ge}, and σ at selected temperatures, shown in Figs. 6–8, clearly indicate how scattered they are. Cirrus cloud microphysical properties are, in general, determined by a number of parameters, including temperature, water vapor mixing ratio, number concentration of cloud particle-forming nuclei, updraft velocity, particle fall velocity, and turbulence and entrainment. The radiative properties of cirrus are, in turn, determined by their microphysical properties. The broad frequency of occurrence distributions in Figs. 6–8 illustrate that factors other than temperature also play important roles in determining cirrus microphysical and radiative properties. This feature also reveals the limitations of the statistics and parameterizations based on small samples.

The frequency distributions of IWC broaden with increasing temperature (Fig. 6), though they have similar shapes. However, there are clear differences in Fig. 7 between the frequency distributions of D_{ge} according to temperature. With a decrease of temperature, the D_{ge} distribution becomes narrower and the modal value of D_{ge} decreases. At -25°C the distribution is flatter than the other selected temperatures because particles in this temperature are exposed to different environmental conditions, which can produce large particles by rapid growth or aggregation processes and small particles by breakup from evaporation. The differences between the frequency distributions of σ (Fig. 8) are smaller than those for IWC and D_{ge}. Because σ depends on IWC/D_{ge}, the temperature dependencies of IWC and D_{ge} compensate for each other to some extent in the σ temperature dependency.

b. *Temperature and thickness dependencies of layer-integrated or mean properties*

As Figs. 6–8 demonstrate, temperature is not the only parameter that controls cirrus cloud microphysical and radiative properties. Therefore, we further explore the two-dimensional dependencies of layer-integrated and mean cloud properties on both temperature and thickness. Contours of IWP as a function of ΔZ and T_m (Fig. 9a) indicate that IWP depends on both variables. Note

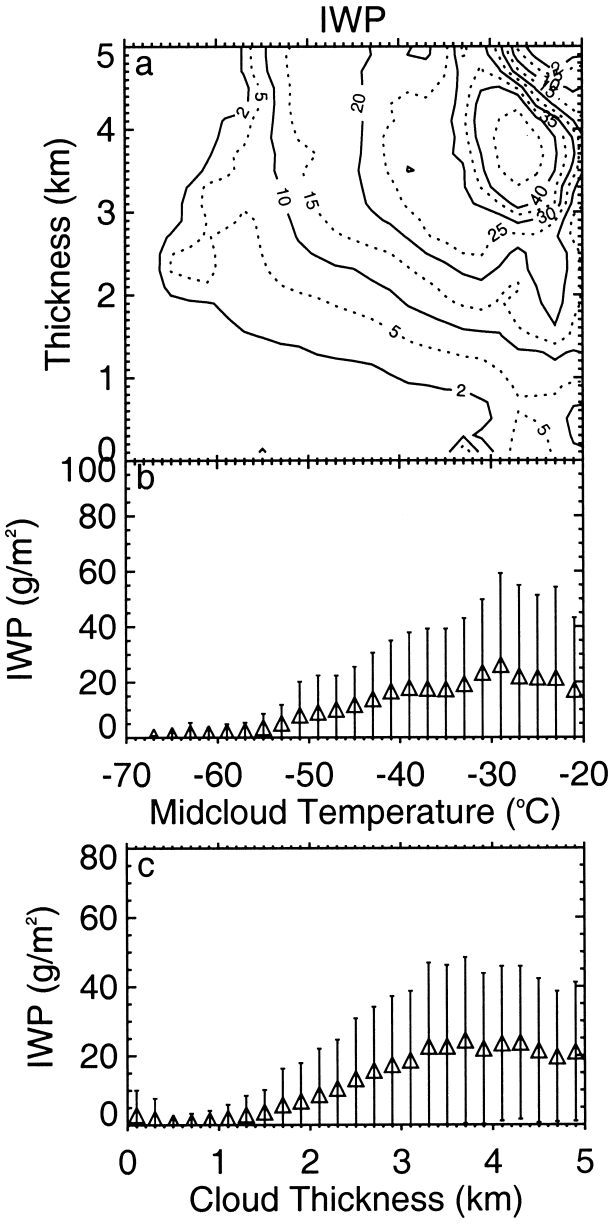

FIG. 9. (a) A contour plot of IWP as functions of T_m and ΔZ, (b) dependency of IWP on T_m (with standard deviations), and (c) dependency of IWP on ΔZ (with standard deviations).

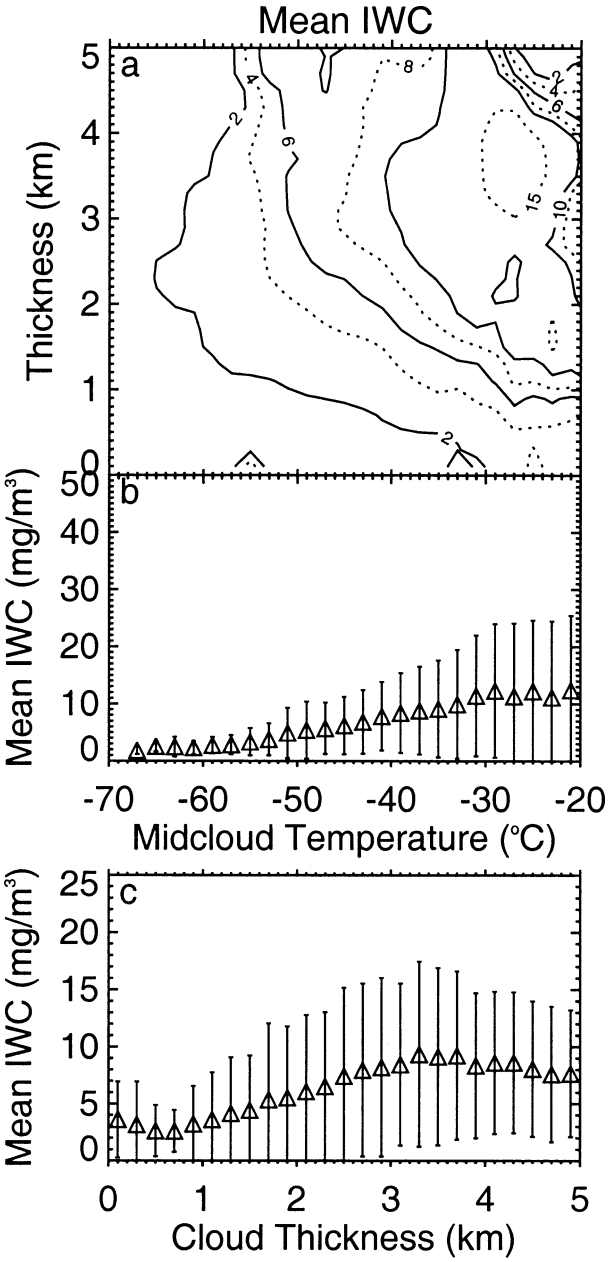

FIG. 10. As in Fig. 9, except for IWC.

that the results around the four corners of the contour plot are not statistically robust due to the limited number of samples in these regions. The mean and standard deviations of IWP as functions of T_m and ΔZ are shown in Fig. 9b and 9c. Mean IWP increases with T_m and ΔZ, although the standard deviation appears too large to allow an accurate parameterization of IWP. Cloud IWP is not very sensitive to cloud thickness for $\Delta Z > 3.5$ km (Fig. 9c), which is also apparent in the contour plot. Similar features for layer-mean IWC are shown in Fig. 10.

The layer mean D_{ge} as a function of ΔZ and T_m is given in Fig. 11a. From the slope of the contours, we can see that D_{ge} is more sensitive to T_m than to ΔZ, which is also revealed by the plots in Figs. 12b and 12c. In contrast to IWP and IWC, the standard deviation of D_{ge} is relatively small, though it is still over 50% of the mean value in most of the data.

Figure 12 depicts the two-dimensional dependency of τ on T_m and ΔZ. This figure reveals that cirrus radiative properties are also sensitive to both T_m and ΔZ, except for the measurements within the upper-right corner of the contour plots. For comparison purposes, the mean cirrus radiative properties from FARS as functions of

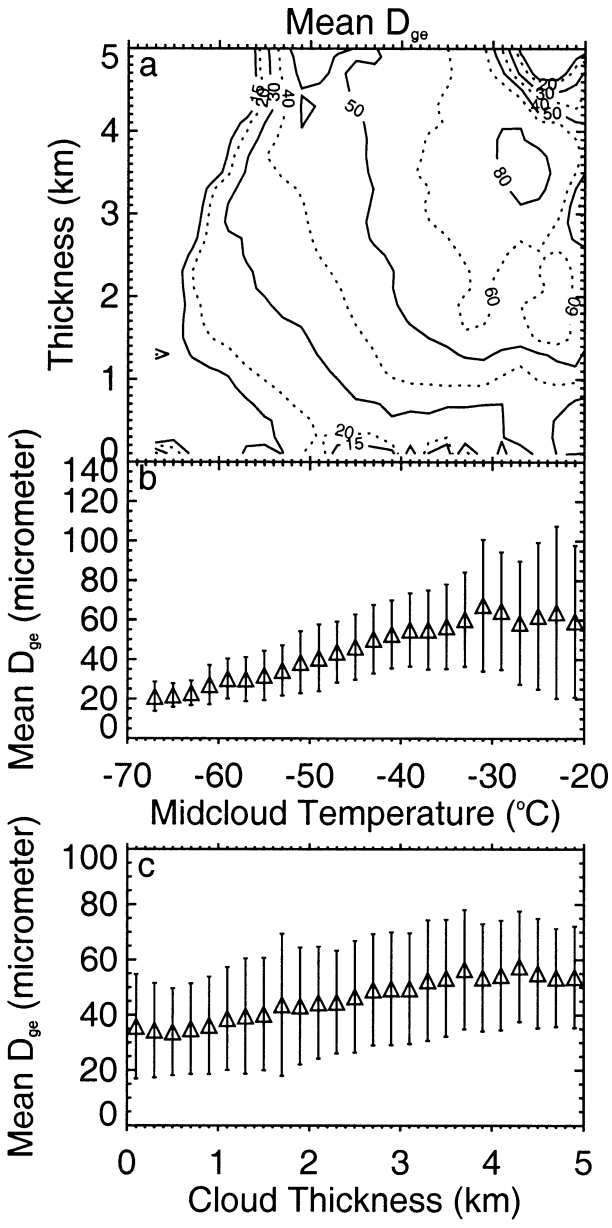

FIG. 11. As in Fig. 9, except for D_{ge}.

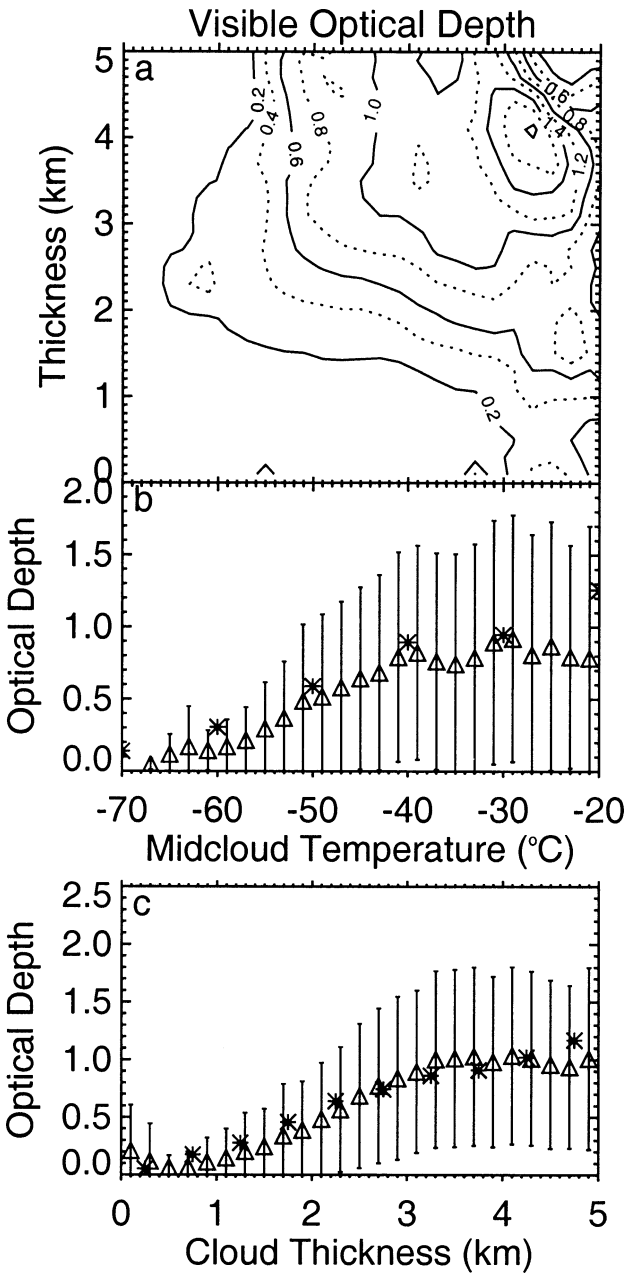

FIG. 12. As in Fig. 9, except for τ. In (b) and (c) the same statistics for FARS cirrus clouds are indicated with asterisks.

cirrus T_m and ΔZ are indicated with an asterisk in Figs. 12b–c. It is noteworthy that the mean cirrus τ at two different continental midlatitude sites have similar temperature and thickness dependencies.

5. Discussion

Various GCMs implement different cloud parameterizations, which lead to different feedbacks between the cloud and hydrological cycle, and between cloud and radiative processes. Remote sensing–derived cloud microphysical and macrophysical properties provide an important source of information to better understand cloud feedbacks, to validate cloud parameterizations in GCMs, and to develop more accurate physically based cloud parameterizations.

Two types of cloud parameterizations, diagnostic and prognostic, are widely used in current GCMs. In diagnostic cloud parameterizations, cloud optical properties are parameterized as a function of temperature (McFarlane et al. 1992). The results in this study provide reliable temperature dependencies of cirrus microphysical and radiative properties for this type of parameterization. However, our results indicate that cloud tem-

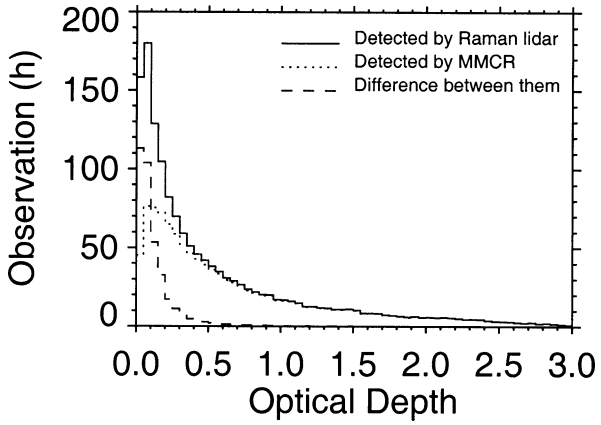

FIG. 13. Frequency distributions in hours of observation for τ for the cirrus clouds detected by the Raman lidar, the MMCR, and their difference during the same period.

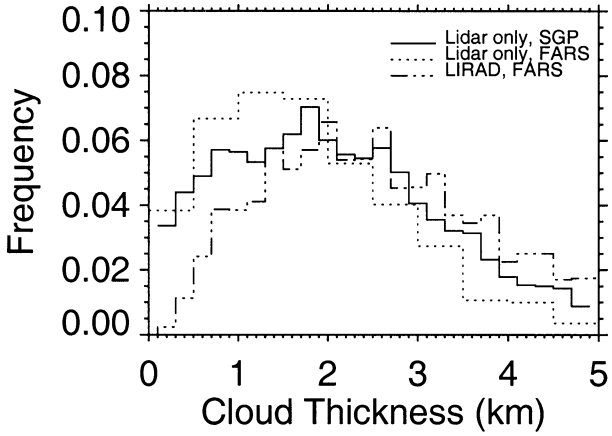

FIG. 14. Frequency distributions of cirrus cloud thickness derived from the Raman lidar (solid line) at the CART SGP site, compared with lidar-only statistics at FARS (dotted line). The statistics from a subset of measurements at FARS, to which the LIRAD algorithm has been applied, is also plotted.

perature itself is not enough to properly parameterize cirrus properties, and temperature-based parameterization can result in serious errors in estimating the cirrus radiative properties. Our calculations show that the solar transmittance of clouds calculated with mean τ is smaller than that calculated with the observed frequency distribution of τ at a given T_m, and that the differences strongly depend on T_m and solar zenith angle. The simplicity of diagnostic cloud parameterizations limits their ability to treat cloud properties correctly, hence GCMs based on these parameterizations most likely have errors in their cloud properties and cloud feedbacks.

A major advantage of using prognostic equations for condensed species is that the cloud optical properties can be parameterized as functions of the predicted cloud water and ice paths, allowing a direct coupling between the hydrological cycle and radiative processes (Fowler et al. 1996). Comparing our cirrus results with the frequency distributions of the effective radius of high-level ice clouds given by Del Genio et al. (1996) and those of water content at different temperatures given by Tiedke (1993), it is clear that predicted cirrus microphysical properties in GCMs are far from realistic. The performance of prognostic cloud parameterizations is limited by many factors, one of which is the inadequate observation of cloud properties (Del Genio et al. 1996). Another limitation is that all parameterizations must contain arbitrary tuning parameters, and the parameterization performance strongly depends on the selection of these parameters (Fowler and Randall 1996; Zurovac-Jevtic 1999). Cirrus properties retrieved from CART observations, as discussed here, show several ways to improve cloud parameterizations, including the selection of tuning parameter values by comparing similar statistics between observations and GCM simulations.

The prognostic cloud parameterization approach is physically realistic, and the various feedbacks involving clouds can be directly expressed in the parameterization. However, the accuracy of the parameterization with this approach depends critically on the realistic treatment of the advective transport of cloud properties, subgrid-scale processes, and cloud microphysical and optical properties. More detailed analysis of retrieved results can help us to better understand the role of different processes in cirrus formation (Mace et al. 2001). A more advanced understanding of these factors is important to developing more physically realistic cloud parameterizations for GCMs.

Cloud radars fail to detect some clouds containing only small particles, which is true even for the MMCR. Distributions of cirrus cloud τ, for cirrus detected by the Raman lidar and the MMCR, for τ bin sizes of 0.05 are presented in Fig. 13. From this figure, we can see

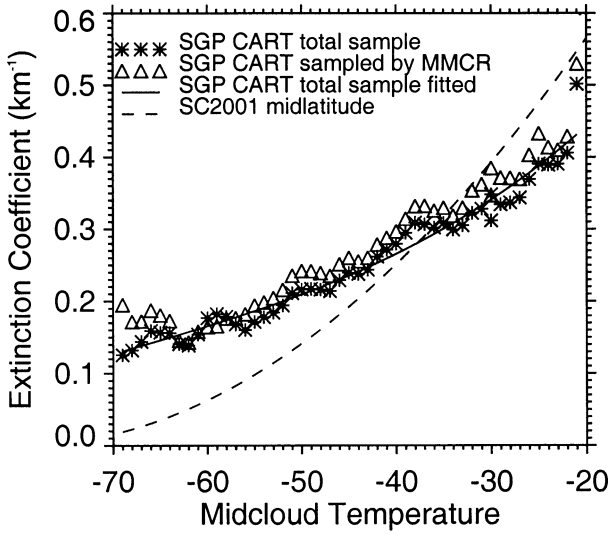

FIG. 15. The dependencies of σ with T_m from the SGP CART cirrus cloud dataset, compared with the parameterization of Sassen and Comstock 2001 (SC2001 midlatitude).

that the MMCR misses most cirrus with $\tau \leq 0.1$. Therefore, cirrus cloud statistics based on radar alone will neglect these optically thin clouds. The main difference in macrophysical properties derived separately from lidar and radar measurements is shown in the frequency distribution of ΔZ in Fig. 2.

Cloud thickness statistics derived from the SGP CART Raman lidar are compared in Fig. 14 with similar statistics from FARS based on lidar-only (Sassen and Campbell 2001) and LIRAD (Sassen and Comstock 2001) measurements. The differences between the FARS and SGP lidar-only results may reflect geographical differences in the cirrus clouds sampled. (Recall that the SGP lidar-only dataset includes optically thin cirrus clouds that the MMCR failed to detect.) The ΔZ statistics of the FARS LIRAD dataset are similar to those of the SGP dataset (Fig. 2a), to which the lidar–radar algorithm has been applied. This indicates that both the lidar–radar and LIRAD methods had difficulty in dealing with optically and/or physically thin cirrus because of signal noise and sensitivity issues. When thin cirrus clouds are omitted by the algorithms, this results in some differences in the frequency of occurrence distributions of cirrus properties, as shown, for example, in Fig. 13 for τ.

The parameterization for σ of Sassen and Comstock (2001) is compared with results from our dataset in Fig. 15. To show the effect of missing some thin cirrus clouds in the statistics, the temperature dependency of layer-mean σ derived from all samples detected by the Raman lidar and from the subset detected also by the MMCR are compared in Fig. 15. These results show that the differences at most temperatures are within 0.02 km^{-1}, with significant differences only for temperatures below $-65°C$ because of the high frequency of thin cirrus at low temperatures. Thus, missing some thin cirrus clouds only slightly affects the temperature and thickness dependencies of cirrus microphysical and radiative properties. The Sassen and Comstock (2001) parameterization, however, has significant differences with the mean properties that we derived from the SGP CART site dataset. An important reason for the difference is caused by the form of the equation used in the parameterization, which forces $\sigma \rightarrow 0$ at a temperature of $-80°C$ as in Platt and Harshvardhan (1988). The layer-mean σ, as a function of T_m from our results, without any temperature constraint, is fitted as $\sigma = 0.7516 + 1.969 \times 10^{-2} T_m + 2.348 \times 10^{-4} T_m^2 + 1.156 \times 10^{-6} T_m^3$, which is plotted as the solid line in the figure.

6. Conclusions

The lidar–radar algorithm developed in Part I has been applied to ~1000 h of SGP CART remote sensing observations, generating one of the most comprehensive cirrus microphysical and radiative property datasets to date. The statistics of cirrus cloud properties and their temperature and thickness dependencies have been described in detail. Our main findings for the SGP CART varieties of midlatitude cirrus clouds are as follows.

1) The frequency distributions of IWP, τ, and layer mean IWC show, as expected, that most cirrus clouds are optically thin with low IWP and a modal value of mean D_{ge} between 30–50 μm. The seasonal changes for these properties are relatively small, except for D_{ge}.
2) Strong temperature dependencies of IWC, D_{ge}, and σ are found and can be fitted well with second-order polynomial functions. However, these properties vary widely at a given temperature as shown by their standard deviations and frequency distributions. These results indicate that factors other than temperature play important roles in regulating cirrus microphysical and radiative properties, and that parameterizations based on small data samples are likely to contain significant errors.
3) The two-dimensional dependencies of IWP, layer-mean IWC, D_{ge}, and τ as functions of midcloud temperature and cloud thickness show that cirrus properties depend on both variables in complicated ways.
4) The frequency distributions of cirrus properties and their dependencies on temperature and thickness are similar at FARS and SGP CART sites. However, the FARS cirrus cloud dataset based on the LIRAD approach appears to be optically thicker (Fig. 3b) because of the limitations of this method when dealing with optically thin clouds (Sassen and Comstock 2001). This results in the relatively large differences in the frequency distributions of cloud properties between the datasets, in contrast to small differences in their temperature and thickness dependencies, as shown in the comparisons.
5) New parameterizations of cirrus properties as a function of T_m are provided, which have differences with prior parameterizations based on ground-based remote sensing and in situ measurements.
6) Comparisons between Raman lidar and MMCR data show that this sensitive cloud radar fails to detect most thin cirrus ($\tau \leq 0.1$) and consistently underestimates cloud thickness. Consequently, there will be a systematic bias in the statistics of cirrus properties based purely on radar data, even for state-of-the-art millimeter wave radar measurements. Caution should be applied to cirrus cloud datasets that rely solely on radar measurements.

Applying these algorithms to additional observations at other CART sites will provide valuable databases to study variations in cirrus cloud microphysical and radiative properties in different climate regimes. These properties can be used to validate and improve cirrus cloud parameterizations in GCMs, and combined with other data, to improve our understanding of cloud physics. We believe that progress is being made in finding an optimal way to parameterize cirrus clouds in GCMs. However, despite the demonstrated usefulness of lidar–

radar algorithms, they can not retrieve cirrus microphysical properties in the presence of low or middle level clouds, which typically block lidar probing, or be applied to thin, cold cirrus clouds. The current algorithms can also be improved with more advanced knowledge concerning the size distributions, shape, bulk density, and backscattering properties of the ice crystals inhabiting cirrus clouds.

Acknowledgments. Our algorithm development research has been supported by the Office of Biological and Environment Research of the U.S. Department of Energy under Grant DEFG0394ER61747 as part of the Atmospheric Radiation Measurement program, and by NASA Grant NAS7-1407 from the CloudSat program. We thank the reviewers for their comments.

REFERENCES

Ansmann, A., U. Wandinger, M. Riebesell, C. Weitkamp, and W. Michaelis, 1992: Independent measurement of extinction and backscatter profiles in cirrus clouds by using a combined Raman elastic-backscatter lidar. *Appl. Opt.,* **31,** 7113–7131.

Cess, R. D., and Coauthors, 1990: Intercomparison and interpretation of climate feedback processes in 19 atmospheric general circulation models. *J. Geophys. Res.,* **95,** 16 601–16 615.

Comstock, J. M., and K. Sassen, 2001: Retrieval of cirrus radiative and backscattering properties using combined lidar and infrared radiometer (LIRAD) measurements. *J. Atmos. Oceanic Technol.,* **18,** 1658–1673.

Del Genio, A. D., M.-S. Yao, W. Kovari, and K. K.-W. Lo, 1996: A prognostic cloud water parameterization for global climate models. *J. Climate,* **9,** 270–304.

Ferrare, R. A., S. H. Melfi, D. N. Whiteman, K. D. Evans, and R. Leifer, 1998: Raman lidar measurements of aerosol extinction and backscattering. Part 1. Methods and comparisons. *J. Geophys. Res.,* **103** (D16), 19 663–19 672.

Fowler, L. D., and D. A. Randall, 1996: Liquid and ice cloud microphysics in the CSU general circulation model. Part III: Sensitivity to modeling assumptions. *J. Climate,* **9,** 561–586.

——, ——, and S. A. Rutledge, 1996: Liquid and ice cloud microphysics in the CSU general circulation model. Part I: Model description and simulated microphysical processes. *J. Climate,* **9,** 489–529.

Fu, Q., 1996: An accurate parameterization of the solar radiative properties of cirrus clouds for climate models. *J. Climate,* **9,** 2058–2082.

Goldsmith, J., B. Forest, S. Bisson, and D. Turner, 1998: Turn-key Raman lidar for profiling atmospheric water vapor, clouds, and aerosols. *Appl. Opt.,* **37,** 4979–4990.

Heymsfield, A. J., and C. M. Platt, 1984: A parameterization of the particle size spectrum of ice clouds in terms of the ambient temperature and the ice water content. *J. Atmos. Sci.,* **41,** 846–855.

Khvorostyanov, V. I., and K. Sassen, 1998: Cirrus cloud simulation using explicit microphysics and radiation. Part II: Microphysics, vapor and ice mass budgets, and optical and radiative properties. *J. Atmos. Sci.,* **55,** 1822–1845.

Liou, K. N., 1986: Influence of cirrus cloud on weather and climate processes: A global perspective. *Mon. Wea. Rev.,* **114,** 1167–1199.

Lohmann, U., and E. Roeckner, 1995: Influence of cirrus cloud radiative forcing on climate and climate sensitivity in a general circulation model. *J. Geophys. Res.,* **100,** 16 305–16 323.

Mace, G. G., E. E. Clothiaux, and T. P. Ackerman, 2001: The composite characteristics of cirrus clouds: Bulk properties revealed by one year of continuous cloud radar data. *J. Climate,* **14,** 2185–2203.

McFarlane, N. A., G. J. Boer, J. P. Blanchet, and M. Lazare, 1992: The Canadian Climate Centre Second-Generation General Circulation Model and its equilibrium climate. *J. Climate,* **5,** 1013–1044.

Moran, K. P., B. E. Martner, M. J. Post, R. A. Kropfli, D. C. Welsh, and K. B. Widener, 1998: An unattended cloud-profiling radar for use in climate research. *Bull. Amer. Meteor. Soc.,* **79,** 443–455.

Platt, C. M. R., and Harshvardhan, 1988: Temperature dependence of cirrus extinction: Implications for climate feedback. *J. Geophys. Res.,* **93,** 11 051–11 058.

——, J. C. Scott, and A. C. Dilley, 1987: Remote sounding of high clouds. Part VI: Optical properties of midlatitude and tropical cirrus. *J. Atmos. Sci.,* **44,** 729–749.

Sassen, K., and J. R. Campbell, 2001: A midlatitude cirrus cloud climatology from the facility for atmospheric remote sensing. Part I: Macrophysical and synoptic properties. *J. Atmos. Sci.,* **58,** 481–496.

——, and J. M. Comstock, 2001: A midlatitude cirrus cloud climatology from the Facility for Atmospheric Remote Sensing. Part III: Radiative properties. *J. Atmos. Sci.,* **58,** 2113–2127.

——, J. M. Comstock, Z. Wang, and G. G. Mace, 2001: Cloud and aerosol research capabilities at FARS: The Facility for Atmospheric Remote Sensing. *Bull. Amer. Meteor. Soc.,* **82,** 1119–1138.

Stephens, G. L., S. Tsay, P. W. Stackhouse, and P. J. Flatau, 1990: The relevance of the microphysical and radiative properties of cirrus clouds to climate and climatic feedback. *J. Atmos. Sci.,* **47,** 1742–1753.

Stokes, G. M., and S. E. Schwartz, 1994: The Atmospheric Radiation Measurement (ARM) program: Programmatic background and design of the Cloud and Radiation Testbed. *Bull. Amer. Meteor. Soc.,* **75,** 1201–1221.

Tiedtke, M., 1993: Representation of clouds in large-scale models. *Mon. Wea. Rev.,* **121,** 3040–3061.

Wang, Z., and K. Sassen, 2001: Cloud type and property retrieval using multiple remote sensors. *J. Appl. Meteor.,* **40,** 1665–1682.

——, and ——, 2002: Cirrus cloud microphysical property retrieval using lidar and radar measurements. Part I: Algorithm description and comparison with in situ data. *J. Appl. Meteor.,* **41,** 218–229.

Young, S. A., 1995: Analysis of lidar backscatter profiles in optically thin clouds. *Appl. Opt.,* **34,** 7019–7031.

Zurivac-Jevtic, D., 1999: Development of a cirrus parameterization scheme: Performance studies in HIRLAM. *Mon. Wea. Rev.,* **127,** 470–485.